About the step-flow mechanism at the origin of graphene crystallisation at the surface of catalysts

Jean-Luc Maurice, Didier Pribat, Zhanbing He, Gilles Patriarche, Costel Sorin Cojocaru

About the step-flow mechanism at the origin of graphene crystallisation at the surface of catalysts

J.-L.Maurice,[a] D. Pribat,[b] Z.He,[a,c] G. Patriarche[d] and C. S. Cojocaru[a],

The nucleation and growth of multiwall carbon nanotubes (MWCNTs) at the surface of crystalline iron-based catalysts are studied by *in situ* annealing and high-resolution transmission electron microscopy. Graphene planes, parallel to the catalyst surface, appear by a mechanism of step flow, where the atomic layers of catalyst are "replaced" by graphene layers. More interestingly, as the catalyst particles have curved or poly-faceted surfaces, those catalyst atomic layers correspond to no definite atomic plane. The step height may thus vary along a given step flow process. Step bunching due to impeded step migration, in certain growth conditions, yields characteristic catalyst nail-head shapes. Mastering this mechanism opens up the way to tailor the structure of MWCNTs, e.g. with highly parallel carbon walls.

Introduction

Graphene, carbon nanofibres (CNFs)[1] or multiwall carbon nanotubes (MWCNTs), obtained by catalytic crystallisation on metallic substrates or particles, have numerous prospects in applications[2-7] but still suffer from irregular – and irreproducible – crystalline structure. The purpose of the present work is to shed some light on the atomic mechanisms that are at work during the crystallisation of graphene layers at the surface of iron-based catalysts, to finally propose routes for the controlled growth of CNTs/CNFs. In the cases of Ni[8-10] and Co[11] catalyst nanoparticles, the nucleation and growth of graphene layershas been shown to rely upon the dynamics of surface steps. The growth of MWCNTs with iron-basedcatalysts has been studied *in situ* ondifferent scales:*in situ* XRD experiments[12, 13]have for instance brought important results on the phase of the catalyst during growth.However, studies at the atomic scale have yet brought little data on the role of atomic steps in the nucleation and growth of graphene.For instance, Rodriguez-Manzo and co-workers[14] have emphasised the role of steps in the nucleation of CNTs from Co, Fe and FeCo (1:1 alloy) nanoparticles using *in situ* high resolution transmission electron microscopy (HRTEM); however they did not study step flow on the catalysts' surface.Yoshida *et al.*[15] have observed the growth of MWCNTs on cementite particles (Fe_3C) *in situ* in HRTEM, but did not focus on atomic-scale nucleation of graphene layers.Begtrup*et al.*[16] have studied Fe faceting during CNT growth, but they have not emphasized the role of steps although they have observed considerable roughening of the catalyst facets where the CNT is generated.

In their seminal paper,Helveg*et al.*have studied Ni-catalysed CNF growth using *in situ* environmental transmission electron microscopy (ETEM)[8]. They were the first to clearly show graphene nucleation at step edges on the lateral walls of the catalyst particles.Nucleation was followed by the receding of the metal steps towards the leading and trailing edges of the metal particle, leaving behind a graphene layer. Movements of metallic matter thus promoted graphene growth on the surface terraces of the catalyst and concomitant elongation of the catalyst particle.

We focus here on the geometry and atomic complexity of those metal steps on the surface of iron-based nanoparticles. We show that, during CNT/CNF growth from Fe-based particles, these steps travel along the entire curved or faceted surface of the catalyst. Thus, they dynamically adapt themselves to the varying local surface orientation. At the end of their trip along the surface, they may eventually form bunches, which induce some characteristic and familiar shapes of catalysts observed after growth. Mastering this step bunching process could open up the way to a better structural control of CNTs and CNFs.

Experimental

The present growth experiments were carried out *in situ* in the transmission electron microscope (TEM), on catalyst particles around which a nanofibre had already developed during a previous direct-current plasma-enhanced chemical vapour deposition (dc-PECVD) growth in a home-made reactor[17]. Transmission electron microscopy observations were done in a Topcon 002B microscope working at 160 kV (point resolution of 0.2 nm). Some *in situ* experiments were performed in a Philips CM30 instrument working at 300 kV (0.23 nm), using a Gatan Model 652 heating sample holder. Finally, for the *in situ*
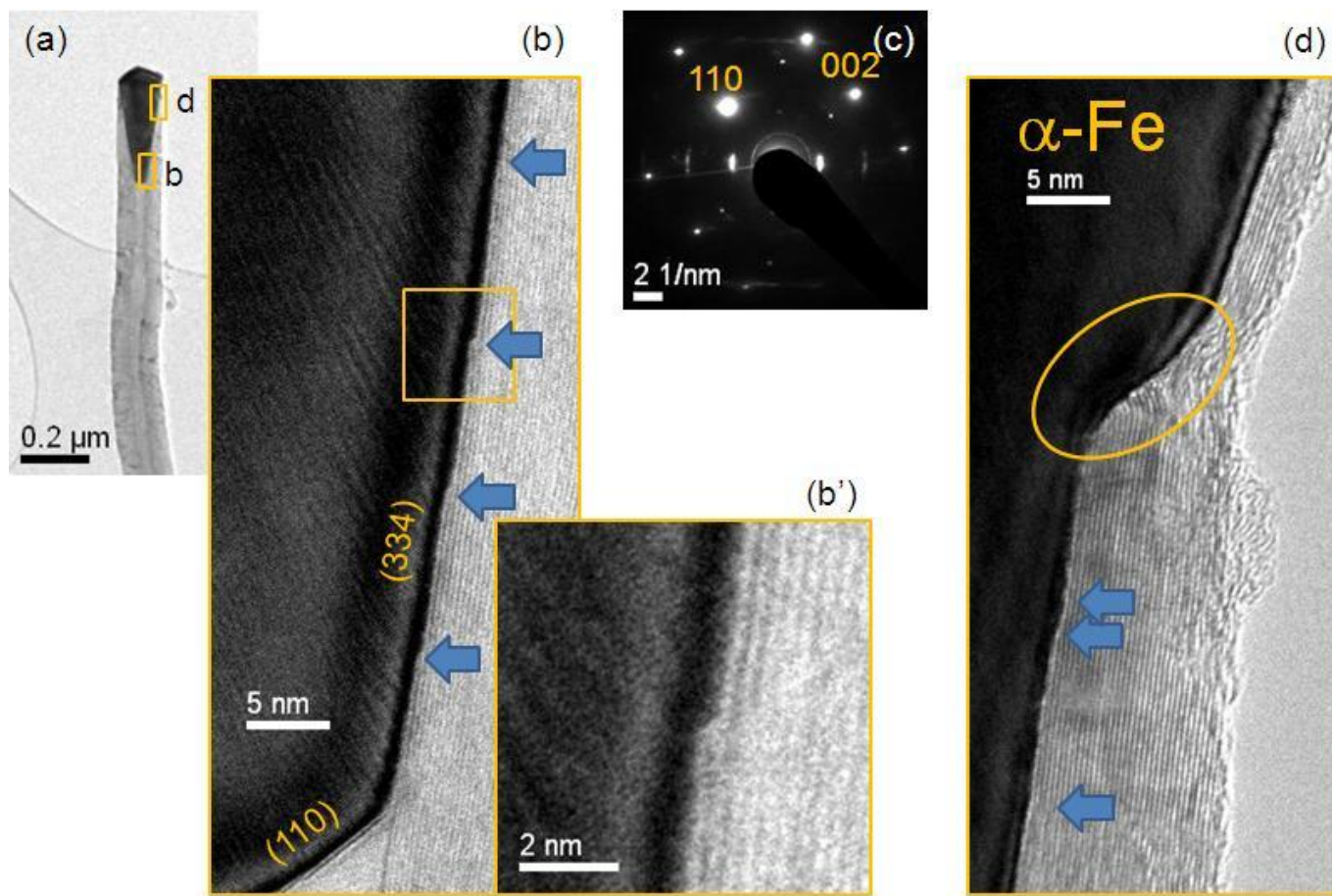
Figure 1. TEM images of a carbon nanofibre obtained with α-Fe catalyst by dcPECVD at 700 °C. a) Low-magnification image; b) and d) high magnification images of respectively the tail and head part of the right-hand side of the catalyst. Blue arrows indicate steps in the catalyst surface that give birth to single graphene layers; b') enlargement of a step in b). (c) Diffraction pattern showing that the catalyst is α-Fe in [1-10] zone axis; a (110) facet can be seen at the tail in b); the (334) surface is probably not a real facet, but just the local orientation of the cone-shaped particle in the [1-10] projection. The circle in d) highlights the inverse shoulder that forms due to step bunching.

HRTEM experiments, we used a Jeol 2200FS microscope working at 200 kV (0.19 nm resolution) equipped with a Protochips Aduro heating sample holder.

In order to dispose of a source of carbon atoms inside the electron microscope, we either amorphised the existing nanotube by electron irradiation[18] or used the carbon present – or injected[14] – in iron carbide catalysts. Similar experiments were performed by Rodriguez-Manzo *et al.*[14] for electron-beam assisted CNT growth inside the TEM, by Ichihashi *et al.*[19], for growth from an amorphous feedstock, and also by Sun *et al.*[20], for growth from irradiated iron carbide.

We focus here on multiwall carbon nanotubes or nanofibres that have a direct application in actual field emission devices[2]. Direct-current plasma-enhanced chemical vapour deposition allows one to obtain the verticality mandatory for field emission applications[1, 21]. The gas mixture we used for growth was made of isopropyl alcohol, water vapour and hydrogen; see details in ref.[17]. We focus on iron-based catalysts because that metal allows one to play with three types of catalysts: α-Fe, γ-Fe and iron carbides[13, 17]. Also, compared to nickel, it appears to favour in certain conditions the growth of real MWCNTs, where the graphene layers are parallel to the tube axis[22].

We note that during such a dc-PECVD growth, the CNTs/CNFs have their catalyst particle on top, so that growth beneath the particle remains shielded from the bombardment of incoming plasma species. Moreover, the growth of each new graphene layer is protected from the outside atmosphere by the already formed layers beneath which it develops. Thus the nucleation and growth processes are quite characteristic of the catalyst surface rather than of the details of the gases or plasma conditions. Hence, reproducing a growth experiment in the TEM with no gas (as we do here) remains a valid approach for the general understanding of growth mechanisms, as long as one sticks to the atomic phenomena at work at the catalyst surface.

Observations

When observed in the TEM, as-grown CNFs often exhibit features that look like the remnants of a growth by a step flow mechanism. In the one with a α-Fe catalyst particle, shown in Fig. 1, the start of a new graphene plane always corresponds to a step on the metal surface (blue arrows in Fig. 1b). The orientation of the metal steps towards the tail of the catalyst and

the existence of an inversed shoulder beneath the head of the particle (Fig. 1d, yellow circle) tend to imply that the steps have been moving during growth, and that they have somehow gathered to form the inversed shoulder. We shall come back later on this inversed shoulder, leading to a "nail head" shape which is a distinctive characteristic of PECVD-grown CNTs/CNFs.

Step migration and bunching upon heat treatment are well known in surface studies[23]; however here, they present two remarkable and original features: (*i*) they are intimately related with the nucleation and growth of graphene, as shown in ref.8 for a Ni catalyst and (*ii*), the steps have non trivial atomic structure on the metal side, as they are on a faceted conical surface[24] and their height, although it depends upon the metal atomic structure, is monitored by the graphite interlayer spacing. This means that the catalyst surface layer that gives birth to graphene by receding may include one or several catalyst crystallographic planes, depending on the local facet plane. The present steps are along a (334) surface, which is most probably just the local orientation of an otherwise cone-shaped surface.

Figure 2 shows the *in situ* growth at 650°C of a proto-nanotube starting from amorphous carbon feedstock[22]. A part of the catalyst particle (which we call sub-nanoparticle in the following) adopts a round-faceted shape on the side where nucleation and growth of the proto-nanotube occurs. This is consistent with previous observations[14, 16]. Due to the formation

of the rounded sub-nanoparticle, iron atoms have to migrate away, starting up a creep mechanism that presently leads to forming a sort of corona around the nanotube (see supplementary information, Fig. S1).

The graphene layers appear to "replace" a volume formerly occupied by α-Fe. The carbon atoms from the amorphous feedstock are incorporated inside the metal by a ring-shaped surface of the catalyst's head, which progressively becomes the corona (supplementary information, Figs. S1 & S2). They may travel to the surface schematized in Fig. 3e either following a transport path along the sidewalls of the particle (at the interface with the encapsulating graphene layers) as described by Begtrup[16], or by direct bulk diffusion[14], the carbon diffusion coefficient in α-Fe being very high at 650 °C[17] (See schematic of C-diffusion in Suppl. Info., Fig. S2).

While some C atoms have to diffuse all the way up to the tip of the sub-nanoparticle, to feed the nucleation and development of new graphene layers (such as those schematised in Fig. 3e), most of them feed the growth of the already developed external walls of the protonanotube, at the bottom part of the sub-nanoparticle.

Let us now give some details on the structures of the protonanotube and its catalyst (Fig. 3). The analysis of the selected-area electron diffraction patterns (EDPs) and their comparison with a real-space image in Fig. 3 indicates that the development of the first graphene layers has provoked a {110} faceting of the Fe sub-nanoparticle. We note, however, that
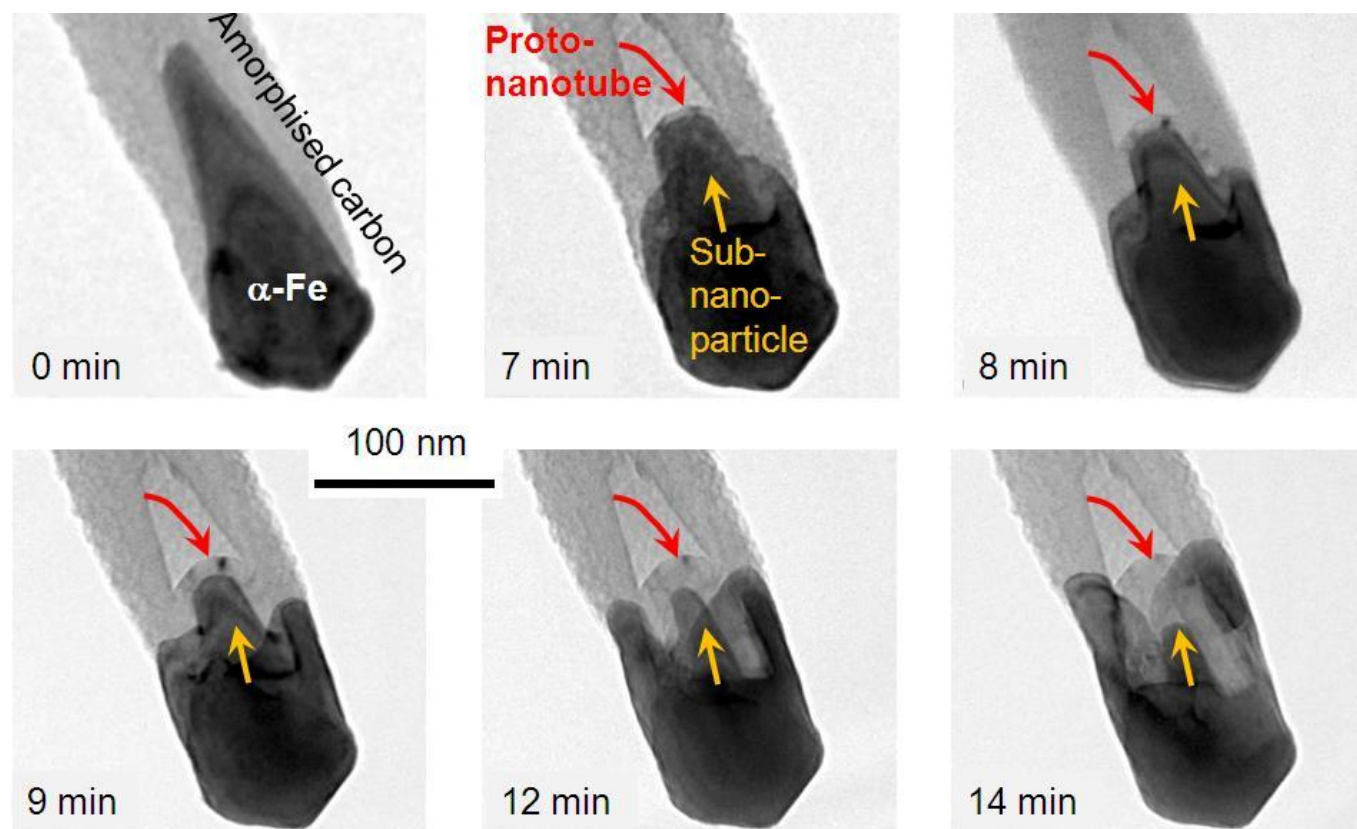

Figure 2. TEM images of a carbon nanofibre first obtained with α-Fe catalyst by dcPECVD at 650 °C[22]. The fibre has been amorphised at room temperature by irradiation with a focused 300 keV electron beam[18, 19], during 30 min, then annealed *in situ* at 650°C, during the time indicated. The arrows are positioned at the same place in all micrographs, to serve as markers. During annealing, the sub-nanoparticle shrinks and elongates while the proto-nanotube thickens by its interior, as if Fe atoms in the α-Fe lattice were being replaced by C atoms in the graphene lattice. After 14 min, the shrinkage leads the sub-nanoparticle to unstick from the protonanotube, which stops the thickening of the latter (see also Supplementary Information, Fig. S1).

these facets have then disappeared when the sub-nanoparticle further shrunk (Fig. 2, 12 min and 13 min). This transient character would explain why the faceting of the catalyst surface in contact with graphene is often not visible in *ex-situ* grown samples[25, 26].

Quite remarkably, the large shape evolution of the Fe catalyst implied neither phase change nor orientation shift (see electron diffraction patterns in Fig. 3 a-b). This is another
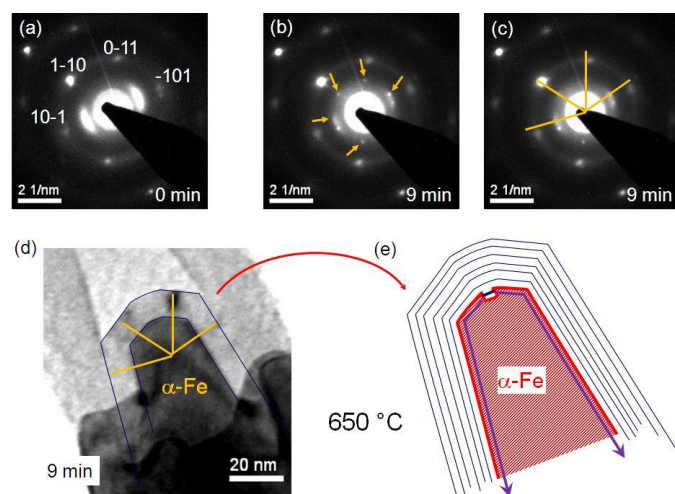

Figure 3. Structure of the protonanotube and its catalyst presented in Fig. 2. a-c) Electron diffraction patterns (EDPs) recorded over an area of 300 nm around the catalyst: a) at the beginning of the 650°C treatment; b and c) after 9 min at that temperature (same EDP with different marks). The main reflections in the pattern show that the catalyst particle is an α-Fe single crystal viewed in [111] zone axis. These reflections remain unchanged during the 9 min while the particle undergoes the significant change of shape visible in Fig. 2: creep of the Fe atoms does not affect the original phase and orientation. After 9 min at 650°C (b and c), individual 002 graphite reflections become clearly visible (arrows in b), indicating the growth of graphite nanocrystals along preferred orientations: their (0002) planes are approximately aligned with the {110} iron planes. Drawing these preferred orientations in (c) and reporting them in direct space (image in d), confirms that they correspond (i) to a{110} faceting of the Fe catalyst and (ii) to a concomitant faceting of the protonanotube. d,e) Image and corresponding schematic diagram of the protonanotube after 9 min of growth. The correlation between the faceting of the sub-nanoparticle and that of the protonanotube clearly appears. Apossible step flow that would allow for the observed catalyst shrinkage (Fig. 2) is indicated by arrows in e).

indication that the change in shape is rather governed by surface motion of atoms/steps and not by a bulk reorganisation. After 9 min of growth the protonanotube was thus also facetted, with facets parallel to Fe {110} facets. Figure 3e gives an example of how a graphene nucleation spot could initiate a step flow responsible for the shrinkage observed in Fig. 2.

In order to confirm such an atomic mechanism with observations on an atomic scale, we carried out the annealing experiment in a high-resolution microscope. Figure 4 shows a lattice-resolved sequence of a similar nanotube formation at the surface of an iron carbide particle.

The Fourier transform of the image of the catalyst delivers a pattern that can be fitted with the [411] diffraction pattern of the metastable Fe_2C phase (suppl. Info., Fig. S3). This phase has higher carbon content than the more stable cementite Fe_3C, which could favour carbon release to the benefit of new graphene layers. Again here, the faceting of the Fe-based particle evolves as graphene layers are generated, with the emergence of surface roughness in facets where graphene layers are being generated(arrows in Figs. 4c &d). Let us note that, while the temperature remains relatively low, the system presents a remarkable efficiency by producing one new graphene layer every 6 seconds. During the development of each new layer, the catalyst surface steps have to cross facet edges (circle in Fig. 4 c,d), thus adapting their structure to each new facet orientation.

The step flow results in a net transport of catalyst matter, which finally modifies, quite strongly, facet surfaces and the catalyst shape in general. It is quite remarkable that, during such a significant evolution, the catalyst mono-crystalline structure remains apparently unchanged.
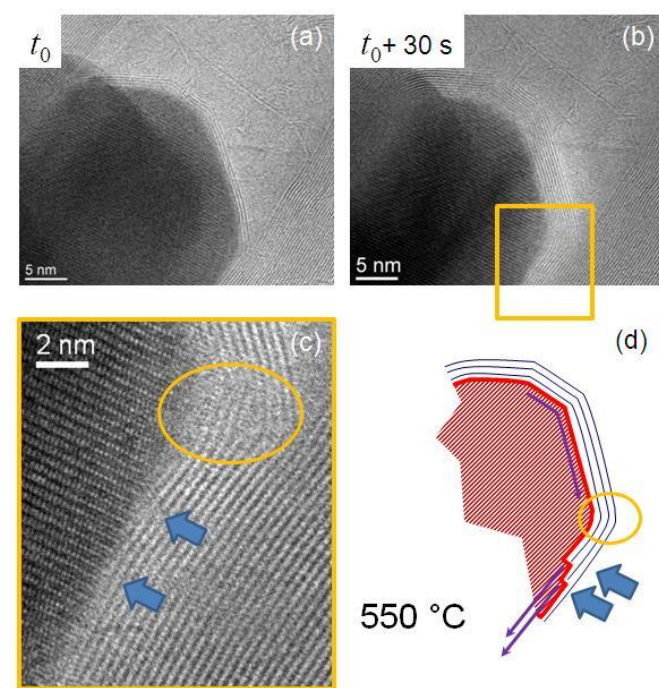

Figure 4. HRTEM images of a carbon nanofibre first obtained with iron carbide catalyst by dcPECVD at 650 °C. a) The nanofibre has been annealed *in situ* for t_0= 4 min 40s at 550°C. b) After 30 additional seconds at 550°C, six graphene layers have developed at the expense of an equivalent volume of the carbide catalyst. c) Enlargement of the yellow rectangle in b) showing the surface steps that give birth to the graphene layers (blue arrows). Those steps induce a roughening of the surface, as well as the defects in the graphene layers due their crossing of facet edge (circle). d) Schematic showing the most likely movement of the steps (purple arrows).

Discussion: an incommensurate mechanism

We now discuss the structural relationships between graphene and metallic substrate. We find that there is no real in-plane matching between graphene and the different catalyst surfaces observed. For instance in the case of α-Fe, graphene growth

appears to promote {110} faceting (Fig. 3). Such facets, the densest in the body-centred cubic structure, are also the lowest energy ones. When calculating the energies of different α-Fe surfaces with one graphene layer lying parallel to them, Begtrup *et al.* found that {110} facets again had the lowest energy[16]. It seems that the step flows at catalyst surface generate atomic movements that help the catalyst surface to reach its lowest energy configuration, while staying in the solid state. However, that lowest-energy configuration presents no remarkable structural match between the catalyst and graphene layers: the symmetriesare different on either side of the interface, the best fitting configuration (between end-on {110} planes in graphite and iron) rests with a 5.1% mismatch, and the step height on the iron side is 0.202 nm (for one single atomic step) or 0.404 nm (for a step of two atomic planes) to be compared with 0.341 nm forthe separation between two consecutive graphene layers.

The example of iron carbide, although less simple due to a more complicated atomic structure, leads to the same conclusions: there is no geometrical correlation between graphene layers and the atomic structure of the catalysts. Graphene layer growth generates or maintains facets on the catalysts but this is not to obtain a given match between the layers and the catalyst. It is most probably because the step-induced atomic movements, generated at the catalyst surface by graphene layer growth, allow the former to reach a minimum energy configuration. Growth of graphene on iron-based catalysts is definitely incommensurate.

Conclusions

The three examples given above are illustrations of the "knitting" of graphene crystal layers by withdrawal of metallic matter (due to receding of surface steps), leaving behind its carbon content in the form of graphene. We had previously observed this mechanism at work during the growth of few-layered graphene on Ni thin films[27, 28]. The present observations uncover a remarkable property of that phenomenon, which is its incommensurate nature. We show indeed that there is no epitaxial-like matching between the growing graphene and the catalyst. Such an observation indicates that, after the graphene has crystallised, the interaction between graphene and catalyst is low.We also note that the surfaces of the catalyst locally reach the low energy configurations of *free surfaces*. Finally, we found that the catalyst surface steps may smoothly move from one catalyst facet to the next, across facet edges, with no rupture in the graphene "knitting" process.

A key point, however, is that of the final destination of the catalyst steps. In any situation, the migration of those steps reshapes the catalyst particle. For instance, in Figs 2 and 3, step migration thins down the sub-nanoparticle while seeding the growth of the protonanotube. A special situation is observed during dcPECVD growth, where the "nail head" shape of the catalyst after growth is a characteristic feature. Here, step migration all around the particle is probably blocked by the ion bombardment on the plasma-exposed surface, leading to step bunching which creates the shoulder also observed in Fig. 1c. Note that in this situation, a first stage of growth must involve

the step flow discussed here, which thins down the bottom part of the catalyst. In a second stage however, no new graphene layers are created, only those already existing continue to grow, eventually leading to the geometry of real MWCNT. In such a geometry, where graphene layers are parallel to the tube axis[17], all the graphite planes making up the nanotube now grow at the same time.

In the framework of applications involving electrical conductivity, like the field emission of interest here, that geometry should drastically decrease the nanotube resistance as conductivity along the planes in graphite is four orders of magnitude better than across the planes.

Notes and references

[a] Laboratoire de Physique des Interfaces et des Couches Minces, LPICM, UMR 7647, CNRS- École Polytechnique, Route de Saclay, 91128 Palaiseau Cedex, France.
[b] Department of Energy Science, Sungkyunkwan University Suwon 440-746, Korea.
[c]State Key Laboratory for Advanced Metals and Materials, University of Science and Technology Beijing, No. 30 Xueyuan Road, Haidian District, Beijing 100083, China.
[d]Laboratoire de photonique et de nanostructures, LPN, UPR 20, CNRS, Route de Nozay, 91460 Marcoussis, France.

1. A. V. Melechko, V. I. Merkulov, T. E. McKnight, M. A. Guillorn, K. L. Klein, D. H. Lowndes and M. L. Simpson, *J. Appl. Phys.*, 2005, **97**.
2. K. B. K. Teo, E. Minoux, L. Hudanski, F. Peauger, J.-P. Schnell, L. Gangloff, P. Legagneux, D. Dieumegard, G. A. J. Amaratunga and W. I. Milne, *Nature*, 2005, **437**, 968-968.
3. L. Bokobza, *Polymer*, 2007, **48**, 4907-4920.
4. L. D. Zhang and M. Fang, *Nano Today*, 2010, **5**, 128-142.
5. X. M. Ren, C. L. Chen, M. Nagatsu and X. K. Wang, *Chem. Eng. J.*, 2011, **170**, 395-410.
6. H. Haniu, N. Saito, Y. Matsuda, T. Tsukahara, Y. Usui, N. Narita, K. Hara, K. Aoki, M. Shimizu, N. Ogihara, S. Takanashi, M.

Okamoto, S. Kobayashi, N. Ishigaki, K. Nakamura and H. Kato, *Journal of Nanomaterials*, 2012.

7. J. M. Schnorr and T. M. Swager, *Chem. Mater.*, 2010, **23**, 646-657.
8. S. Helveg, C. López-Cartes, J. Sehested, P. L. Hansen, B. S. Clausen, J. R. Rostrup-Nielsen, F. Abild-Pedersen and J. K. Nørskov, *Nature*, 2004, **427**, 426-429.
9. S. Hofmann, R. Sharma, C. Ducati, G. Du, C. Mattevi, C. Cepek, M. Cantoro, S. Pisana, A. Parvez, F. Cervantes-Sodi, A. C. Ferrari, R. Dunin-Borkowski, S. Lizzit, L. Petaccia, A. Goldoni and J. Robertson, *Nano Lett.*, 2007, **7**, 602-608.
10. M. Lin, J. P. Y. Tan, C. Boothroyd, K. P. Loh, E. S. Tok and Y. L. Foo, *Nano Lett.*, 2007, **7**, 2234-2238.
11. H. W. Zhu, K. Suenaga, A. Hashimoto, K. Urita, K. Hata and S. Iijima, *Small*, 2005, **1**, 1180-1183.
12. J. Cambedouzou, P. Landois, S. Rouzière, M. Pinault, C. Mocuta, L. Hennet, D. Thiaudière, M. Mayne-L'Hermite and P. Launois, *Phys. Rev. B*, 2013, **88**, 081402.
13. C. T. Wirth, B. C. Bayer, A. D. Gamalski, S. Esconjauregui, R. S. Weatherup, C. Ducati, C. Baehtz, J. Robertson and S. Hofmann, *Chem. Mater.*, 2012, **24**, 4633-4640.
14. J. A. Rodriguez-Manzo, M. Terrones, H. Terrones, H. W. Kroto, L. T. Sun and F. Banhart, *Nature Nanotechnol.*, 2007, **2**, 307-311.
15. H. Yoshida, S. Takeda, T. Uchiyama, H. Kohno and Y. Homma, *Nano Lett.*, 2008, **8**, 2082-2086.
16. G. E. Begtrup, W. Gannett, J. C. Meyer, T. D. Yuzvinsky, E. Ertekin, J. C. Grossman and A. Zettl, *Phys. Rev. B*, 2009, **79**, 205409.
17. Z. He, J.-L. Maurice, A. Gohier, C. S. Lee, D. Pribat and C. S. Cojocaru, *Chem. Mater.*, 2011, **23**, 5379-5387.
18. A. V. Krasheninnikov and F. Banhart, *Nat Mater*, 2007, **6**, 723-733.
19. T. Ichihashi, J.-I. Fujita, M. Ishida and Y. Ochiai, *Phys. Rev. Lett.*, 2004, **92**, 215702.
20. L. Sun, F. Banhart, A. V. Krasheninnikov, J. A. Rodríguez-Manzo, M. Terrones and P. M. Ajayan, *Science*, 2006, **312**, 1199-1202.
21. M. Chhowalla, K. B. K. Teo, C. Ducati, N. L. Rupesinghe, G. A. J. Amaratunga, A. C. Ferrari, D. Roy, J. Robertson and W. I. Milne, *J. Appl. Phys.*, 2001, **90**, 5308-5317.
22. J. L. Maurice, Z. B. He and C. S. Cojocaru, in *Advances in Imaging and Electron Physics, Vol 179*, ed. P. W. Hawkes, Elsevier Academic Press Inc, San Diego, 2013, vol. 179, pp. 142-144.
23. M. Sussiau, F. Nguyen-Van-Dau, P. Galtier and A. Schuhl, *Appl. Phys. Lett.*, 1996, **69**, 857-859.
24. Z. He, X. Ke, S. Bals and G. Van Tendeloo, *Carbon*, 2012, **50**, 2524-2529.
25. Z. B. He, J.-L. Maurice, C. S. Lee, A. Gohier, D. Pribat, P. Legagneux and C. S. Cojocaru, *Carbon*, 2011, **49**, 435-444.
26. Z. B. He, J.-L. Maurice, C. S. Lee, C. S. Cojocaru and D. Pribat, *AJSE*, 2010, **35**, 19-28.
27. L. Baraton, Z. B. He, C. S. Lee, C. S. Cojocaru, M. Châtelet, J. L. Maurice, Y. H. Lee and D. Pribat, *EPL (Europhys. Lett.)*, 2011, **96**, 46003.
28. L. Baraton, Z. He, C. S. Lee, J.-L. Maurice, C. S. Cojocaru, A.-F. Gourgues-Lorenzon, Y. H. Lee and D. Pribat, *Nanotechnology*, 2011, **22**, 085601.